

CERN-TH/97-325  
hep-ph/9711408  
November 1997

## Squark and Gluino Production at Hadron Colliders <sup>\*</sup>

Michael Spira

*CERN, Theory Division, CH-1211 Geneva 23, Switzerland*

### Abstract

The theoretical status of squark and gluino production at present and future hadron colliders is reviewed. I shall concentrate on the evaluation of SUSY-QCD corrections to the production cross sections and their phenomenological implications.

CERN-TH/97-325  
hep-ph/9711408  
November 1997

---

<sup>\*</sup>Contribution to the proceedings of the *International Workshop on Quantum Effects in the MSSM*, 9–13 September 1997, Barcelona, Spain

# Squark and Gluino Production at Hadron Colliders

MICHAEL SPIRA

*CERN, Theory Division, CH-1211 Geneva 23, Switzerland  
E-mail: Michael.Spira@cern.ch*

The theoretical status of squark and gluino production at present and future hadron colliders is reviewed. I shall concentrate on the evaluation of SUSY-QCD corrections to the production cross sections and their phenomenological implications.

## 1 Introduction

Supersymmetry is a new symmetry between fermions and bosons, which has not been observed so far at the level of elementary particles. The symmetry is motivated by the interest of providing a natural solution to the hierarchy problem due to the absence of quadratic divergences in perturbation theory, in contrast with the Standard Model. Supersymmetric grand unified theories have predicted a Weinberg angle in striking agreement with the present measurements at the electroweak scale. An important constraint of supersymmetric theories is that they predict a light scalar Higgs boson with mass  $M_h \lesssim 130$  GeV.

The search for Higgs bosons and supersymmetric particles provides a strong motivation for present and future experiments. The colored supersymmetric particles, squarks and gluinos, can be searched for at the present Tevatron experiments, a  $p\bar{p}$  collider with a c.m. energy of 1.8 TeV upgraded soon to 2 TeV, and the LHC in the near future, a  $pp$  collider with a c.m. energy of 14 TeV. The Tevatron searches set presently the most stringent mass bounds on these particles: at 95% CL, gluinos have to be heavier than  $\sim 175$  GeV, while squarks with masses below  $\sim 175$  GeV have been excluded for gluino masses  $m_{\tilde{g}} \lesssim 300$  GeV<sup>1</sup>. In  $R$ -parity conserving theories, e.g. the minimal supersymmetric extension of the Standard Model [MSSM], supersymmetric particles can only be produced in pairs. All supersymmetric particles will decay to the lightest one [the LSP], which is stable stable thanks to conserved  $R$ -parity. As a consequence the typical signatures for the production of supersymmetric particles will mainly be jets and missing transverse energy, carried away by the LSP.

Squarks and gluinos can be produced in 4 different processes,

$$p\bar{p}/pp \rightarrow \tilde{q}\tilde{q}, \tilde{q}\bar{\tilde{q}}, \tilde{g}\tilde{g}, \tilde{q}\tilde{g} + X \quad (1)$$

We worked in the approximation of mass-degenerate light-flavored squarks, so that mixing effects are absent. However, this approximation is not valid for

stop production, where mass splitting and mixing effects are sizeable. Stop production has been presented elsewhere<sup>2</sup>. The light quarks ( $u, d, s, c, b$ ) will be treated as massless particles, while the top quark will be included in loops with a mass  $m_t = 175$  GeV. Moreover, stops are taken into account in the virtual loops, too, with a mass equal to the other squark masses. Since their effect will be suppressed, this provides a reasonable approximation. In Eq. 1 a summation over all possible squark flavors and charge conjugate final states should be implicitly understood.

## 2 Lowest Order

The calculation of the lowest order (LO) cross sections of the processes in Eq. 1 was performed a long time ago<sup>3</sup>. The 4 production processes divide into several partonic subprocesses [ $N_F = 5$ ]:

(i)  $qq' \rightarrow \tilde{q}\tilde{q}'$ :

$$\hat{\sigma}_{LO} = \frac{4\pi\alpha_s^2}{9\hat{s}} \left\{ \frac{\hat{s} + 2m_-^2}{\hat{s}} L_1 - \beta_{\tilde{q}} \frac{m_{\tilde{g}}^2 \hat{s} + 2m_-^4}{m_{\tilde{g}}^2 \hat{s} + m_-^4} - \delta_{qq'} \frac{2}{3} \frac{m_{\tilde{g}}^2}{\hat{s} + 2m_-^2} L_1 \right\} \quad (2)$$

(ii)  $gg \rightarrow \tilde{q}\tilde{q}$ :

$$\hat{\sigma}_{LO} = N_F \frac{\pi\alpha_s^2}{\hat{s}} \left\{ \beta_{\tilde{q}} \frac{5\hat{s} + 62m_{\tilde{q}}^2}{24\hat{s}} - \frac{m_{\tilde{q}}^2}{3\hat{s}} \frac{4\hat{s} + m_{\tilde{q}}^2}{\hat{s}} \log \left( \frac{1 + \beta_{\tilde{q}}}{1 - \beta_{\tilde{q}}} \right) \right\} \quad (3)$$

$q\bar{q}' \rightarrow \tilde{q}\bar{\tilde{q}}'$ :

$$\begin{aligned} \hat{\sigma}_{LO} = & \frac{4\pi\alpha_s^2}{9\hat{s}} \left\{ \frac{\hat{s} + 2m_-^2}{\hat{s}} L_1 - \frac{m_{\tilde{g}}^2 + 2m_-^2}{m_{\tilde{g}}^2 + m_-^2} \beta_{\tilde{q}} \right. \\ & \left. + \delta_{qq'} \left[ \frac{\beta_{\tilde{q}}}{3} \left( \frac{1 + 2m_-^2}{\hat{s}} + N_F \frac{\hat{s} - 4m_{\tilde{q}}^2}{\hat{s}} \right) + 2 \frac{m_{\tilde{g}}^2 \hat{s} + m_-^4}{\hat{s}^2} L_1 \right] \right\} \end{aligned} \quad (4)$$

(iii)  $gg \rightarrow \tilde{g}\tilde{g}$ :

$$\hat{\sigma}_{LO} = \frac{3\pi\alpha_s^2}{4\hat{s}} \left\{ 3 \left( 1 - 2 \frac{m_{\tilde{g}}^2}{\hat{s}} \right)^2 \log \left( \frac{1 + \beta_{\tilde{g}}}{1 - \beta_{\tilde{g}}} \right) - \frac{12\hat{s} + 17m_{\tilde{g}}^2}{\hat{s}} \beta_{\tilde{g}} \right\} \quad (5)$$

$q\bar{q} \rightarrow \tilde{g}\tilde{g}$ :

$$\hat{\sigma}_{LO} = \frac{\pi\alpha_s^2}{\hat{s}} \left\{ \left( \frac{20}{27} + \frac{16m_{\tilde{g}}^2}{9\hat{s}} - \frac{8m_-^2}{3\hat{s}} + \frac{32m_-^4}{27(m_{\tilde{g}}^2\hat{s} + m_-^4)} \right) \beta_{\tilde{g}} \right. \\ \left. + \left( \frac{64m_-^2}{27\hat{s}} + \frac{8m_{\tilde{g}}^2}{27(\hat{s} - 2m_-^2)} - \frac{8}{3} \frac{m_{\tilde{g}}^2\hat{s} + m_-^4}{3\hat{s}^2} \right) L_2 \right\} \quad (6)$$

(iv)  $gq \rightarrow \tilde{g}\tilde{q}$ :

$$\hat{\sigma}_{LO} = \frac{\pi\alpha_s^2}{\hat{s}} \left\{ -\frac{\lambda}{9\hat{s}^2} (7\hat{s} + 32m_-^2) + \frac{2m_-^2}{9} \frac{4\hat{s} - m_{\tilde{q}}^2 - m_-^2}{\hat{s}^2} L_3 \right. \\ \left. + \frac{\hat{s}^2 + 2m_-^2\hat{s} - 2m_-^2m_{\tilde{q}}^2}{\hat{s}^2} L_4 \right\} \quad (7)$$

with

$$L_1 = \log \left( \frac{s + 2m_-^2 + \hat{s}\beta_{\tilde{q}}}{s + 2m_-^2 - \hat{s}\beta_{\tilde{q}}} \right) \quad L_2 = \log \left( \frac{s - 2m_-^2 + \hat{s}\beta_{\tilde{g}}}{s - 2m_-^2 - \hat{s}\beta_{\tilde{g}}} \right) \\ L_3 = \log \left( \frac{s - m_-^2 + \lambda}{s - m_-^2 - \lambda} \right) \quad L_4 = \log \left( \frac{s + m_-^2 + \lambda}{s + m_-^2 - \lambda} \right) \\ \beta_{\tilde{q}} = \sqrt{1 - \frac{4m_{\tilde{q}}^2}{\hat{s}}} \quad \beta_{\tilde{g}} = \sqrt{1 - \frac{4m_{\tilde{g}}^2}{\hat{s}}} \\ m_-^2 = m_{\tilde{g}}^2 - m_{\tilde{q}}^2 \quad \lambda = \sqrt{(\hat{s} - m_{\tilde{g}}^2 - m_{\tilde{q}}^2)^2 - 4m_{\tilde{g}}^2m_{\tilde{q}}^2} \quad (8)$$

The LO hadronic cross sections can be obtained by convoluting the partonic ones with the corresponding parton densities. At the Tevatron  $\tilde{q}\bar{\tilde{q}}$  production is the dominant process for squark masses lighter than the gluino mass, while in the reverse case gluino pair production dominates. The associated  $\tilde{q}\tilde{g}$  production process always provides a sizeable fraction of SUSY particle production. Beyond the excluded mass range the  $q\bar{q}$  initial state dominates over the  $gg$  initial state in  $\tilde{q}\bar{\tilde{q}}$  and  $\tilde{g}\bar{\tilde{g}}$  pair production. At the LHC the situation is reversed: for smaller squark masses,  $\tilde{q}\tilde{q}$  and  $\tilde{q}\tilde{g}$  production are dominant, while for larger

squark masses SUSY particle production is dominated by  $\tilde{g}\tilde{g}$  and  $\tilde{q}\tilde{q}$  production. Moreover, the  $gg$  initial state clearly dominates gluino pair production. The LO scale dependence leads to an estimate of  $\sim 50\%$  uncertainty for the production cross sections. Since the reconstruction of squarks and gluinos will be very difficult due to the escaping LSP, an important possibility to measure the squark and gluino masses is provided by the values of the total cross sections. Thus a complete NLO calculation is needed in order to reduce the theoretical errors to a reliable level<sup>4</sup>.

### 3 SUSY QCD Corrections

The evaluation of the SUSY QCD corrections will be exemplified for  $\tilde{q}\tilde{q}$  production. These corrections split into two pieces, the virtual ones, generated by virtual particle exchanges, and the real ones, which originate from gluon radiation and the corresponding crossed processes with three-particle final states.

#### 3.1 Virtual corrections



Figure 1: *Typical diagrams of the virtual corrections.*

The one-loop virtual corrections are built up by gluon, gluino, quark and squark exchange contributions [see Fig. 1]. Their contraction with the LO matrix elements provides the one-loop contributions to the physical matrix elements. The evaluation of the virtual corrections has been performed in dimensional regularization, leading to the extraction of ultraviolet, infrared and collinear singularities as poles in  $\epsilon = (4 - n)/2$ . For the chiral  $\gamma_5$  coupling we have used the naive scheme, which is justified in the present analysis at the one-loop level without anomalies. We have explicitly checked that after summing all virtual corrections no quadratic divergences are left over, in accordance with the general property of supersymmetric theories. The renormalization has been performed by identifying the squark and gluino masses with their pole masses, and defining the strong coupling in the  $\overline{\text{MS}}$  scheme, including five light flavors in the corresponding  $\beta$  function. The massive particles, i.e. squarks, gluinos and top quarks, have been decoupled by subtracting their contribution at vanishing momentum transfer<sup>5</sup>. In dimensional regularization,

there is a mismatch between the gluonic degrees of freedom [d.o.f. =  $n - 2$ ] and those of the gluino [d.o.f. = 2], so that SUSY is explicitly broken. In order to restore SUSY in the physical observables in the massless limit, an additional finite counter-term is required for the renormalization of the novel  $\tilde{q}\tilde{g}\tilde{q}$  vertex<sup>6</sup>.

### 3.2 Real corrections

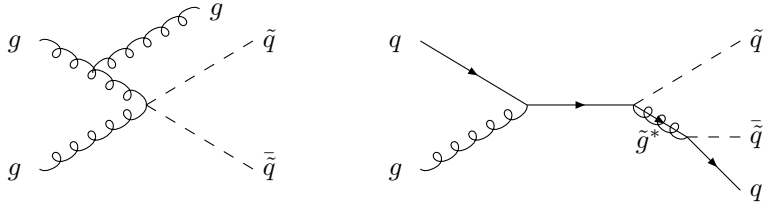


Figure 2: Typical diagrams of the real corrections.

The real corrections originate from the radiation of a gluon in all possible ways and from the crossed processes by interchanging the gluon of the final state against a light quark in the initial state. The phase-space integration of the final-state particles has been performed in  $n = 4 - 2\epsilon$  dimensions, leading to the extraction of infrared and collinear singularities as poles in  $\epsilon$ . In order to isolate the singularities we have introduced a cutoff  $\Delta$  in the invariant mass of, say, the  $\tilde{q}g$  pair, which separates soft and hard gluon radiation. After evaluating all angular integrals and adding the virtual and real corrections, the infrared singularities cancel. The left-over collinear singularities are universal and are absorbed in the renormalization of the parton densities at NLO. We defined the parton densities in the conventional  $\overline{\text{MS}}$  scheme including five light flavors, i.e. the squark, gluino and top quark contributions are not included in the mass factorization. Finally we end up with an ultraviolet, infrared and collinear finite partonic cross section, which is independent of the cutoff for  $\Delta \rightarrow 0$ .

However, there is an additional class of physical singularities, which have to be regularized<sup>4</sup>. In the second diagram of Fig. 2 an intermediate  $\tilde{q}g^*$  state is produced, before the [off-shell] gluino splits into a  $\tilde{q}\tilde{q}$  pair. If the gluino mass is larger than the common squark mass, and the partonic c.m. energy is larger than the sum of the squark and gluino masses, the intermediate gluino can be produced on the mass shell. Thus the real corrections to  $\tilde{q}\tilde{q}$  production contain a contribution of  $\tilde{q}\tilde{g}$  production. The residue of this part corresponds to  $\tilde{q}\tilde{g}$  production with the subsequent gluino decay  $\tilde{g} \rightarrow \tilde{q}\tilde{q}$ , which is already contained in the LO cross section of  $\tilde{q}\tilde{g}$  pair production, including all final-state

cascade decays,

$$\frac{d\sigma_{res}(gq \rightarrow \tilde{g}\tilde{q} \rightarrow \tilde{q}\bar{\tilde{q}}q)}{dp_{\tilde{g}}^2} = \hat{\sigma}(gq \rightarrow \tilde{g}\tilde{q}) BR(\tilde{g} \rightarrow \tilde{q}\bar{\tilde{q}}) \frac{m_{\tilde{g}}\Gamma_{\tilde{g}}/\pi}{(p_{\tilde{g}}^2 - m_{\tilde{g}}^2)^2 + m_{\tilde{g}}^2\Gamma_{\tilde{g}}^2} \quad (9)$$

Thus this term has to be subtracted in order to derive a well-defined production cross section for each individual final state. Analogous subtractions emerge also in other reactions: if the gluino mass is larger than the squark mass, the contributions from  $\tilde{g} \rightarrow \tilde{q}\bar{\tilde{q}}$ ,  $\tilde{q}\bar{\tilde{q}}$  have to be subtracted, and in the reverse case the contributions of squark decays into gluinos have to be subtracted.

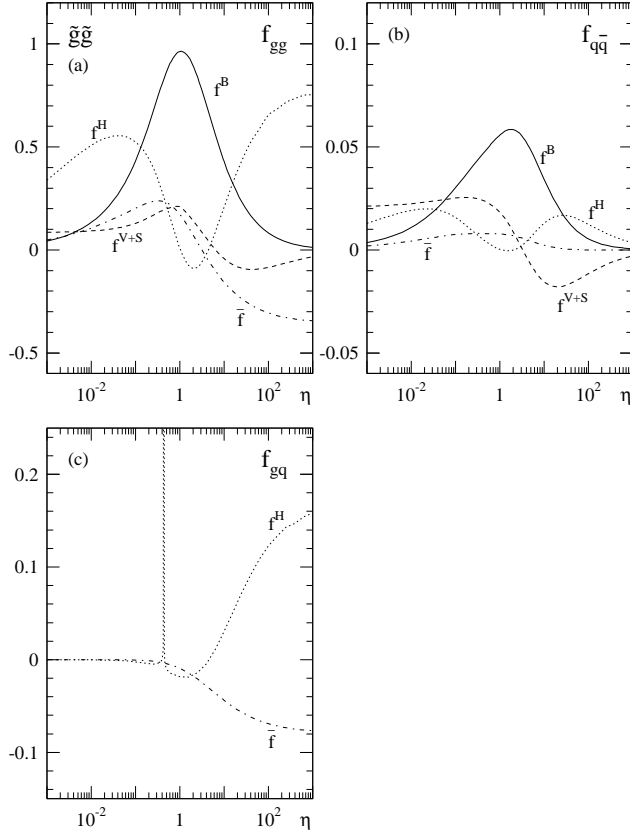


Figure 3: Scaling functions of the gluino pair production cross sections [ $\eta = \hat{s}/(4m_{\tilde{g}}^2) - 1$ ]. Top mass:  $m_t = 175$  GeV.

## 4 Results

### 4.1 Partonic cross sections

The partonic scaling functions are defined as

$$\hat{\sigma}_{ij} = \frac{\alpha_s^2(Q^2)}{m^2} \left\{ f_{ij}^B + 4\pi\alpha_s(Q^2) \left[ f_{ij}^{V+S} + f_{ij}^H + \bar{f}_{ij} \log \frac{Q^2}{m^2} \right] \right\} \quad (10)$$

The parameter  $m$  denotes the average mass of the produced massive particles. The scaling functions are shown for gluino pair production in Fig. 3 as a function of  $\eta = \hat{s}/(4m_g^2) - 1$  for the  $gg$ ,  $q\bar{q}$  and  $gq$  initial states. The singularity of  $f_{gg}$  at  $\hat{s} = (m_{\tilde{q}} + m_{\tilde{g}})^2$  is a left-over singularity of the residue subtraction, which however is integrable<sup>4</sup>. The scaling functions can be evaluated analytically in the threshold region  $\beta \ll 1$  and the high energy limit  $\hat{s} \gg m_{\tilde{q}}^2, m_{\tilde{g}}^2$ .

In the threshold region the dominant contributions originate from Coulomb singularities in the  $f_{ij}^{V+S}$  functions due to Coulombic gluon exchange between the final state particles and from large logarithmic enhancements in the  $f_{ij}^H$  and  $\bar{f}_{ij}$  functions due to soft gluon radiation from the initial states. The leading logarithms of soft gluon radiation can be resummed<sup>7</sup>. The analytic results in the threshold region for e.g.  $gg \rightarrow \tilde{q}\bar{\tilde{q}}$  are given by

$$\begin{aligned} f_{gg}^B &= \frac{7}{192} N_F \pi \beta & f_{gg}^{V+S} &= f_{gg}^B \frac{11}{336\beta} \\ f_{gg}^H &= f_{gg}^B \left\{ \frac{3}{2\pi^2} \log^2(8\beta^2) - \frac{183}{28\pi^2} \log(8\beta^2) \right\} & \bar{f}_{gg} &= -f_{gg}^B \frac{3}{2\pi^2} \log(8\beta^2) \end{aligned} \quad (11)$$

In the high energy region the LO cross sections scale as  $\hat{\sigma}_{LO} \propto \alpha_s/\hat{s}$ , while the NLO cross sections develop a high-energy plateau,  $\hat{\sigma}_{NLO} \propto \alpha_s^2/m^2$ , originating from  $t$ -channel gluon exchange between an initial quark/gluon line and the hard process. Thus the scaling functions  $f_{ij}^H, \bar{f}_{ij}$  approach finite values, which can be calculated by using the factorization in  $k_T$  of the exchanged gluon<sup>8</sup>. For  $\tilde{q}\bar{\tilde{q}}$  pair production the non-zero limits read as

$$\begin{aligned} f_{gg}^H &= \frac{2159}{4320\pi} & f_{gq}^H &= \frac{2159}{19440\pi} \\ \bar{f}_{gg} &= -\frac{11}{72\pi} & \bar{f}_{gq} &= -\frac{11}{324\pi} \end{aligned} \quad (12)$$

#### 4.2 Hadronic cross sections

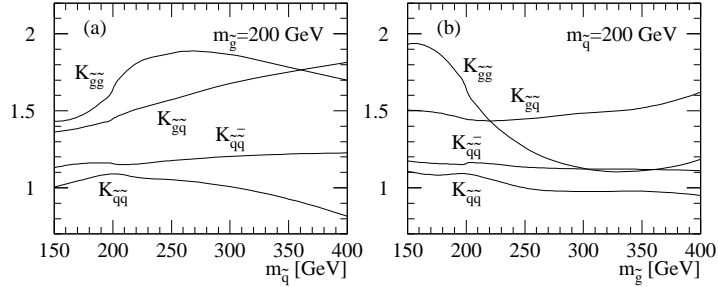


Figure 4: *K* factors of the different squark and gluino production cross sections at the Tevatron. Parton density: GRV(94) with  $Q = m$ . Top mass:  $m_t = 175$  GeV.

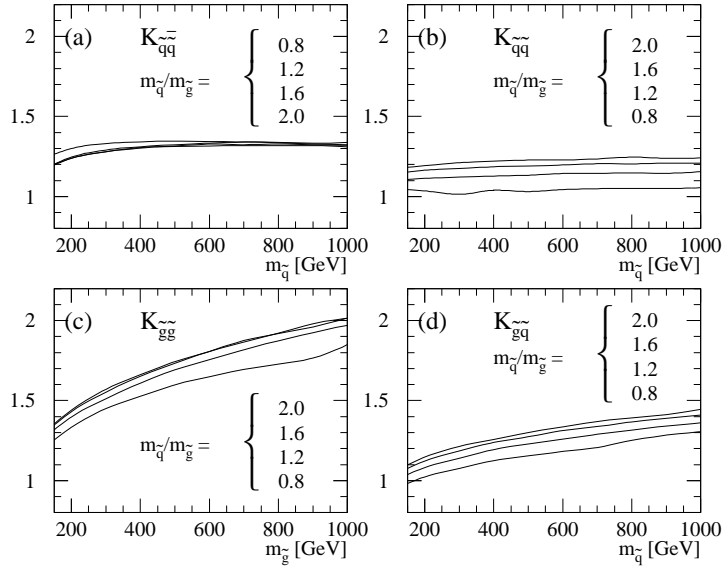


Figure 5: *K* factors of the different squark and gluino production cross sections at the LHC. Parton density: GRV(94) with  $Q = m$ . Top mass:  $m_t = 175$  GeV.

The hadronic cross sections can be obtained by convoluting the partonic ones with the corresponding parton densities. We have performed the numerical analysis for the Tevatron and the LHC. For the natural renormalization/factorization scale choice  $Q = m$ , where  $m$  denotes the average mass of the final-state SUSY particles, the SUSY QCD corrections are large and positive, increasing the total cross sections by 10–90%<sup>4</sup>. This is shown in Figs. 4,5,

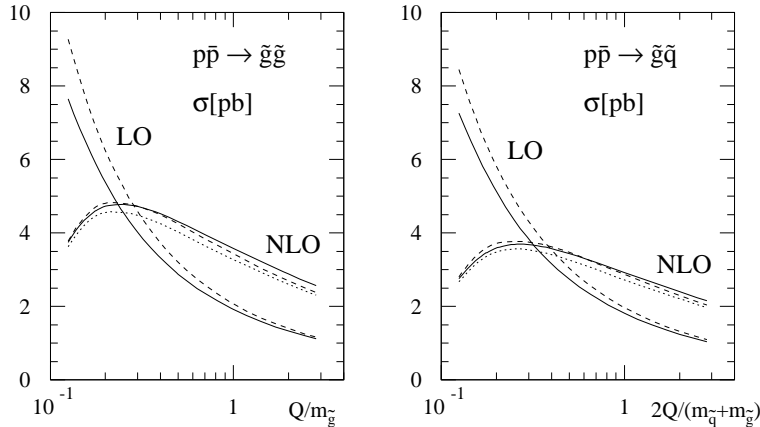


Figure 6: *Scale and parton density dependence of the total  $\tilde{g}\tilde{g}$  and  $\tilde{g}\tilde{q}$  production cross sections at the Tevatron in LO and NLO. Parton densities: GRV(94) (solid), CTEQ3 (dashed) and MRS(A') (dotted); mass parameters:  $m_{\tilde{q}} = 280$  GeV,  $m_{\tilde{g}} = 200$  GeV and  $m_t = 175$  GeV.*

where the  $K$  factors, defined as the ratios of the NLO and LO cross sections, are presented as a function of the corresponding SUSY particle mass for the Tevatron and the LHC.

We have investigated the residual scale dependence in LO and NLO, which is presented in Fig. 6. Including the NLO corrections reduces the LO scale dependence by a factor of 3–4 and reaches a typical level of  $\sim 15\%$ , which serves as an estimate of the remaining theoretical uncertainties<sup>4</sup>. Moreover, the dependence on different sets of parton densities is rather weak and leads to an additional uncertainty of  $\sim 10\%$ <sup>4</sup>. In order to quantify the effect of the NLO corrections on the search for squarks and gluinos at hadron colliders, we have extracted the SUSY particle masses corresponding to several fixed values of the production cross sections. These masses are increased by 10–30 GeV at the Tevatron [see Fig. 7] and by 10–50 GeV at the LHC [see Fig. 8], thus enhancing the present bounds on the squark and gluino masses significantly<sup>4</sup>.

Finally we have evaluated the QCD-corrected transverse-momentum and rapidity distributions for all different processes. As can be inferred from Fig. 9, the modification of the normalized distributions in NLO compared to LO is less than 10% for the transverse-momentum distributions and negligible for the rapidity distributions. Thus it is a sufficient approximation to rescale the LO distributions uniformly by the  $K$  factors of the total cross sections<sup>4</sup>.

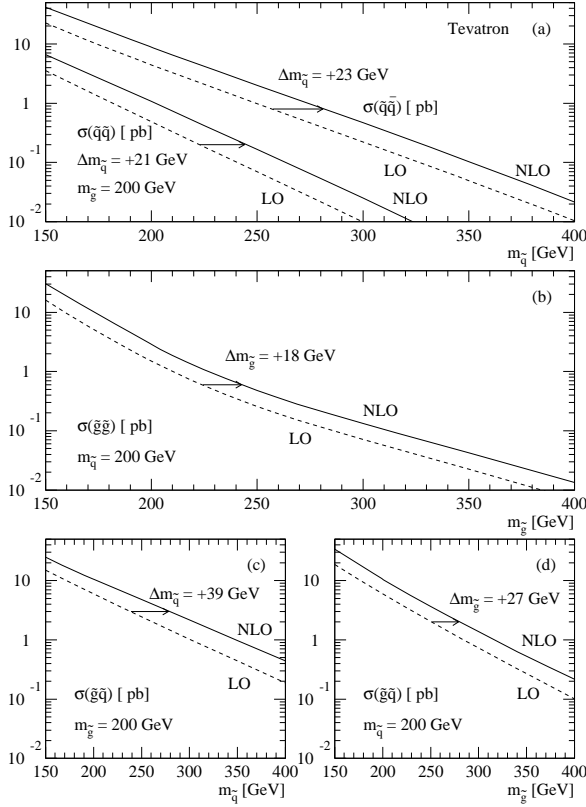


Figure 7: The total cross sections for the Tevatron [ $\sqrt{S} = 1.8$  TeV]. NLO (solid): GRV(94) parton densities, with scale  $Q = m$ ; compared with LO (dashed): EHLQ parton densities, at the scale  $Q = \sqrt{s}$ .

## 5 Conclusions

We have reviewed the theoretical status of the squark and gluino production cross sections at present and future hadron colliders. The evaluation of the full SUSY-QCD corrections has been described in detail. They enhance the cross sections by about 10–90% and are thus significant for a reliable prediction. In spite of the large size of the NLO corrections, the residual scale dependence is reduced by a factor of 2.5–4, so that the theoretical uncertainty decreased to  $\sim 15\%$ . The dependence on different parton densities is  $\sim 10\%$  and thus weak. The NLO corrections increase the bounds on the squark and gluino masses, extracted from upper bounds on the total cross sections, by about 15–35 GeV at the Tevatron and by 10–50 GeV at the LHC. The shape of the

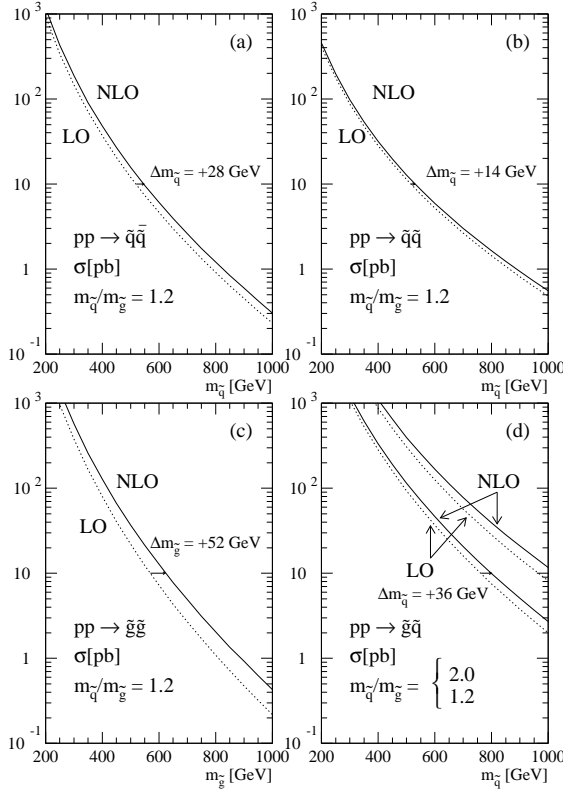


Figure 8: The total cross sections for the LHC [ $\sqrt{S} = 14$  TeV]. NLO (solid) compared with LO (dashed). GRV(94) parton densities, with scale  $Q = m$ .

differential distributions in the transverse momentum  $p_T$  and the rapidity  $y$  are hardly affected by the NLO corrections, so that a simple rescaling of the LO distributions by the  $K$  factors of the total cross sections provides a reasonable approximation within  $\sim 10\%$ . The final results are encoded in the Fortran program PROSPINO<sup>9</sup>.<sup>†</sup>

### Acknowledgements

I would like to thank W. Beenakker, R. Höpker and P. Zerwas for the pleasant collaboration in the work presented here.

<sup>†</sup>PROSPINO is available from <http://wwwcn.cern.ch/~mspira/> and <http://www-lorentz.leidenuniv.nl/wwreport/>.

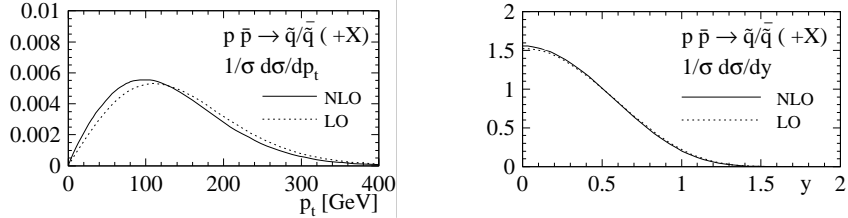


Figure 9: Normalized transverse-momentum and rapidity distributions of  $p\bar{p} \rightarrow \tilde{q}\bar{\tilde{q}} + X$  at the Tevatron in LO (dotted) and NLO (solid). Parton densities: GRV(94) with  $Q = m$ ; mass parameters:  $m_{\tilde{q}} = 280$  GeV,  $m_{\tilde{g}} = 200$  GeV and  $m_t = 175$  GeV.

## References

1. F. Abe et al., CDF-Coll., Phys. Rev. Lett. **75** (1995) 613; S. Abachi et al., D0-Coll., Phys. Rev. Lett. **75** (1995) 618.
2. W. Beenakker, M. Krämer, T. Plehn, M. Spira and P.M. Zerwas, preprint CERN-TH/97-177, hep-ph/9710451; T. Plehn and W. Beenakker, these proceedings.
3. G.L. Kane and J.P. Leveillé, Phys. Lett. **B112** (1982) 227; P.R. Harrison and C.H. Llewellyn Smith, Nucl. Phys. **B213** (1983) 223 [Err. Nucl. Phys. **B223** (1983) 542]; E. Reya and D.P. Roy, Phys. Rev. **D32** (1985) 645; S. Dawson, E. Eichten and C. Quigg, Phys. Rev. **D31** (1985) 1581; H. Baer and X. Tata, Phys. Lett. **B160** (1985) 159.
4. W. Beenakker, R. Höpker, M. Spira and P.M. Zerwas, Phys. Rev. Lett. **74** (1995) 2905, Z. Phys. **C69** (1995) 163, Nucl. Phys. **B492** (1997) 51.
5. J. Collins, F. Wilczek and A. Zee, Phys. Rev. **D18** (1978) 242; W.J. Marciano, Phys. Rev. **D29** (1984) 580; P. Nason, S. Dawson and R.K. Ellis, Nucl. Phys. **B303** (1988) 607.
6. S.P. Martin and M.T. Vaughn, Phys. Lett. **B318** (1993) 331.
7. G.S. Sterman, Nucl. Phys. **B281** (1987) 310; S. Catani and L. Trentadue, Nucl. Phys. **B327** (1989) 323, *ibid.* **B353** (1991) 183.
8. S. Catani, M. Ciafaloni and F. Hautmann, Nucl. Phys. **B366** (1991) 135.
9. W. Beenakker, R. Höpker and M. Spira, hep-ph/9611232.